Superparamagnetic and ferromagnetic Ni nanorod arrays fabricated on Si substrates using electroless deposition

2009 Nanotechnology 20 415703

(http://iopscience.iop.org/0957-4484/20/41/415703)

Nanotechnology **20** (2009) 415703 (7pp) doi:10.1088/0957-4484/20/41/415703

Superparamagnetic and ferromagnetic Ni nanorod arrays fabricated on Si substrates using electroless deposition

Chien-Min Liu[1], Yuan-Chieh Tseng[1], Chih Chen[1,3], Ming-Chieh Hsu[2], Tzu-Yzan Chao[2] and Yu-Ting Cheng[2]

[1] Department of Materials Science and Engineering, National Chiao Tung University, Hsin-chu, 30010, Taiwan, Republic of China
[2] Department of Electronics Engineering, National Chiao Tung University, Hsin-chu, 30010, Taiwan, Republic of China

E-mail: chih@mail.nctu.edu.tw

Received 22 May 2009, in final form 26 August 2009
Published 18 September 2009
Online at stacks.iop.org/Nano/20/415703

Abstract

The microstructures and magnetic properties of nickel nanorods fabricated using an anodic alumina oxide template and electroless deposition were investigated. The as-deposited nanorods were found to contain nanocrystalline grains with an average size of ∼2–3 nm. The temperature-dependent magnetic hysteresis curves indicated superparamagnetic behavior of the as-deposited rods as a result of the reduction of ferromagnetic crystallites. The superparamagnetic (SM) Ni nanorods transformed into ferromagnetic (FM) ones when annealed at 400 °C. Results from dark-field transmission electron microscopy reveal that the microstructure of the rods tends to form a laminar structure with grain growth parallel to the long axis of the rods, together with the enhancement of ferromagnetic ordering along the same direction. The results suggest that the SM–FM phase transition obtained is microstructure driven. The Ni nanorods manufactured by the electroless deposition also have the potential to serve as magnetic building blocks in nanoscale devices, such as high-frequency inductors. On-chip magnetic spiral inductors were fabricated using these nanorods, and it was demonstrated that the nanorods can enhance inductance up to 6 GHz.

(Some figures in this article are in colour only in the electronic version)

1. Introduction

Nanostructured magnetic materials have attracted substantial attention in recent decades because their properties differ markedly from those of their bulk counterparts [1–7]. Their tunable properties make them promising candidates for use in biomedicine, radio frequency (RF) inductors, spintronic devices, and information-storage applications [8–11]. Recent advances in the fabrication of nanostructured magnetic materials, such as by physical vapor deposition, chemical vapor deposition, wet-chemical reaction, electrodeposition, atomic layer deposition and template synthesis, have led to an emergent field that demands more research efforts. In this work, template synthesis was conducted on anodic aluminum oxide (AAO), a template material that has been extensively adopted [12–16]. to grow well shape controlled and highly oriented Ni nanorods [17–20]. Thanks to the excellent orientation control of the AAO, the magnetic properties of the Ni nanorods can be studied in a direction-confined manner. This provides the major advantage of excluding the anisotropy effect upon the magnetic properties while focusing on other aspects, such as microstructure and chemical composition. Differing from most wire- or rod-structure studies of transition metals using electrodeposition on AAO [21, 22], electroless deposition was employed in this work because of its superiority in terms of easy fabrication, low cost and mass production, which bear more advantages for practical applications. However, materials synthesized by electroless deposition were found to exhibit microstructures

[3] Author to whom any correspondence should be addressed.

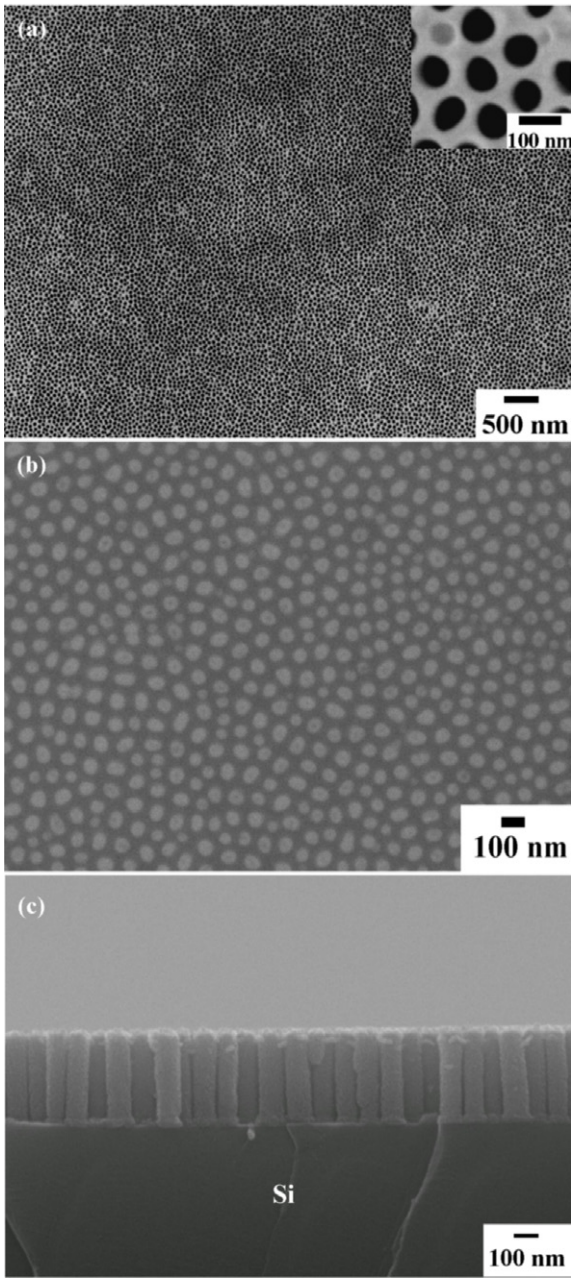

Figure 1. (a) SEM top-view image of surface morphology of AAO template. (b) SEM top-view image of surface morphology of Ni nanorods formed in AAO holes. (c) SEM cross-sectional image of Ni nanorods on a Si substrate.

very distinct from those synthesized by electrodeposition. The former is inclined to form a nanocrystalline structure [23], while the later tends to be polycrystalline [24]. Such a dissimilarity may accordingly modify the magnetic properties, therefore providing a foundation for the development of materials with tailored properties. However, at present, there have been relatively few studies toward this goal.

As motivated by this cause, we present a work in which we investigate a superparamagnetic–ferromagnetic phase transition in Ni nanorods fabricated by electroless deposition. The results demonstrate that the magnetic phase transition is strongly coupled to the change of microstructure, which has never been observed in the electrodeposition. In addition, on-chip magnetic spiral inductors were incorporated with the Ni nanorods in order to demonstrate the potential applications for such nanostructured materials in magnetic devices. The paper is organized as follows. Section 1 is the introduction. Section 2 describes the experimental details. Section 3 contains the results and discussion. Section 4 provides the conclusion.

Table 1. The bath composition and operation parameters for the electroless Ni deposition.

Composition/condition	Specifications
$NiSO_4 \cdot 6H_2O$	20 (g l^{-1})
$NaH_2PO_2 \cdot H_2O$	27 (g l^{-1})
$Na_2C_4H_4O_4 \cdot 6H_2O$	16 (g l^{-1})
$Pb(NO_3)_2$	1 ppm
pH	5.0
Temperature (°C)	65

2. Experimental details

An AAO template with pores of about 70 nm was prepared on a Si substrate by following the process described in [21, 22]. The AAO-Si sample surface was sensitized and activated by a $SnCl_2$/HCl solution (40 g l^{-1} $SnCl_2$ + 3 ml l^{-1} HCl) and a $PdCl_2$/HCl solution (0.15 g l^{-1} $PdCl_2$ + 3 ml l^{-1} HCl) prior to the electroless deposition process. The electroless plating solution used in this work mimicked the recipe described by Tsai *et al* [23] which was composed of a mixture of $NiSO_4$, NaH_2PO_2, $Na_2C_4H_4O_4$ and $Pb(NO_3)_2$, serving as the main Ni source, the reducing agent, the stabilizing agent and the buffer agent, respectively. The operating conditions of the electroless deposition are summarized in table 1, and further details can be found in the literature [23, 25]. The pH value of the plating bath plays an important role in determining the size of the nanocrystals during the electroless deposition, which was adjusted to be ∼5 by dilute aqueous H_2SO_4 in order to compare with the literature [23]. Subsequently, Ni was deposited on the AAO-Si substrate with the described bath conditions, forming a nanorod structure (figure 1(c)) due to the confinement of the AAO. After the deposition was complete, the Ni nanorods were annealed at 400 °C in a N_2 atmosphere for 30 s, 1 min and 2 min. Finally, the AAO was removed by bathing the samples in an NaOH solution, leaving the rods rooted perpendicularly on the Si substrate (figure 1(c)).

The Ni nanorods were characterized by surface morphology, microstructural analysis and magnetic and compositional measurements. The surface morphology was probed using a scanning electron microscope (SEM, JSM 6500F) operated at 15 kV (figure 1). A transmission electron microscope (TEM, JEM-2100F, operated at 200 keV) and high-resolution imaging were used to probe the microstructure (figure 2) and atomic-scale images (figure 3), respectively. The magnetic properties were identified by a superconducting quantum interference device (SQUID) magnetometer (figures 4 and 5), and the magnetizations were all normalized to the saturated one

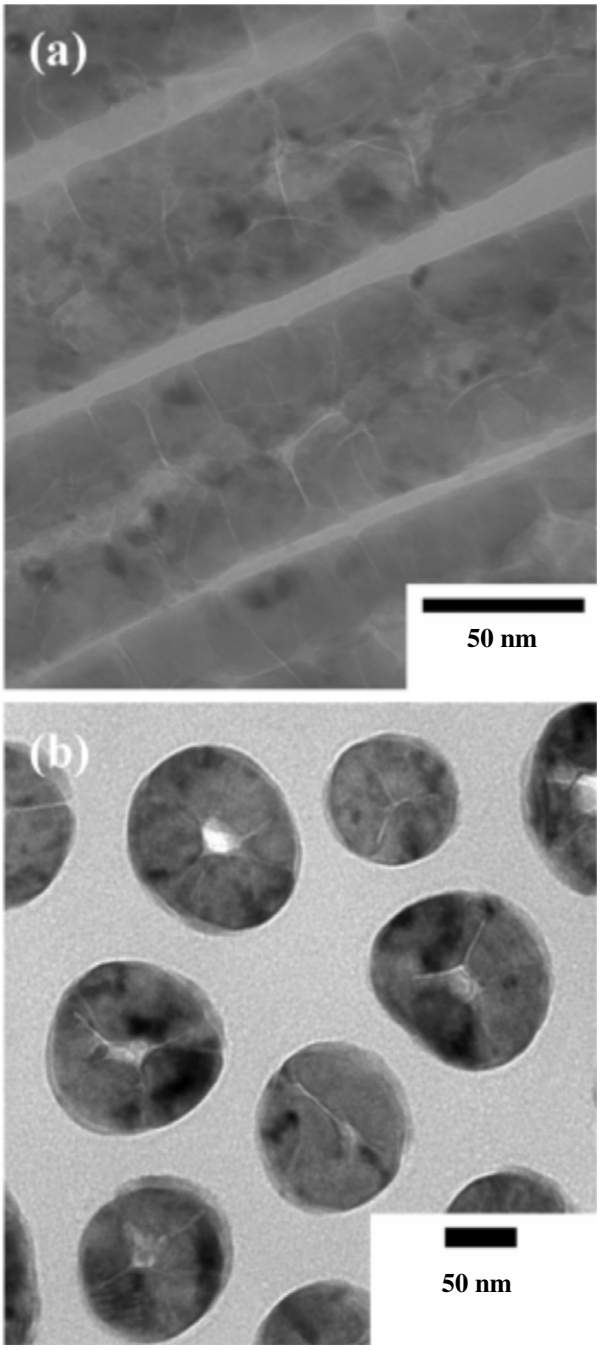

Figure 2. (a) Cross-sectional and (b) top-view TEM images of the as-deposited Ni nanorods.

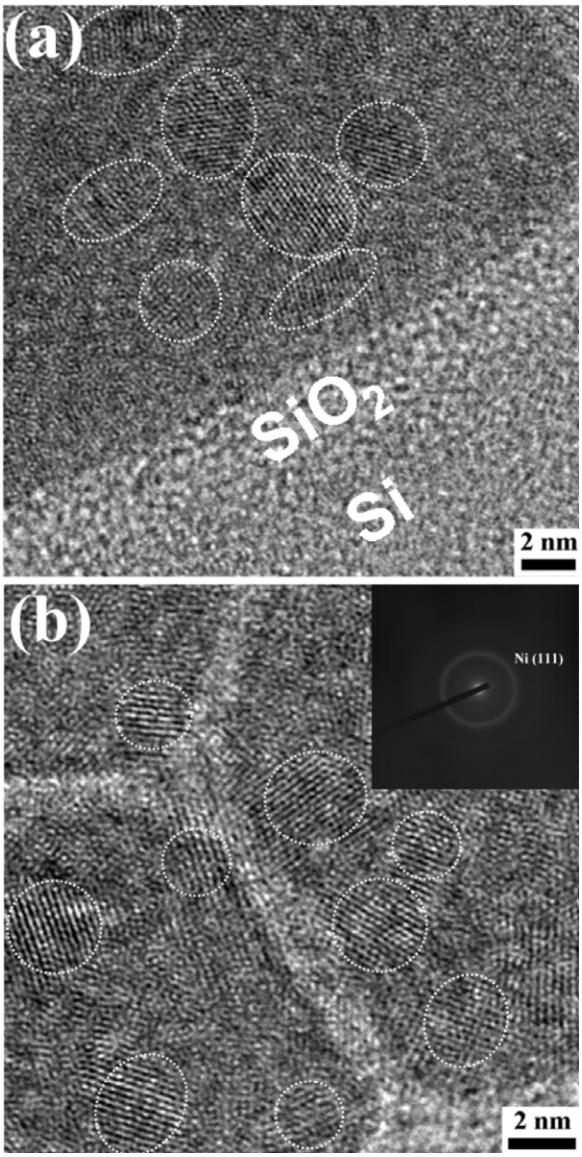

Figure 3. High-resolution TEM images of the as-deposited Ni nanorods. The lattice planes of the nanocrystalline grains are highlighted by dashed circles. (a) The root of the rods planted on the Si substrate with a SiO_2 interlayer. (b) The junction between columnar structures; each column is composed of nanocrystalline grains. Inset: SAED pattern of the Ni nanorods showing a diffusive ring of Ni {111} lattice plane as a result of the nanocrystals.

(M/M_s). The composition of the nanorods was determined by energy-dispersive x-ray spectrometry (EDS), showing the atomic percentages of Ni and P to be 82.1% and 17.9%, respectively. The chemical composition agrees reasonably well with the literature [23].

To investigate the potential applications of the Ni nanorods, spiral inductors were incorporated. The fabrication process of the spiral inductors on top of the Ni nanorods followed the flow charts presented in figure 3 of Hsu *et al* [26]. For inductor characterization, two-port scattering parameters (S-parameters) of the inductors were measured up to 20 GHz with an on-wafer probe station using high-frequency probes (Cascade Microtech, Inc., ACP-40-GSG-100 μm) and an Agilent E8364B PNA network analyzer. The parasitic parallel capacitance between the contact pads of the inductor was de-embedded using the measured result of the designed dummy pattern. The de-embedded S parameters were then transformed into Y-parameters, and the equivalent series inductance (L) of the inductors was extracted from the Y-parameters according to the following equation [43]:

$$L = \mathrm{Im}(1/Y_{11})/2\pi f \tag{1}$$

where f is the signal frequency.

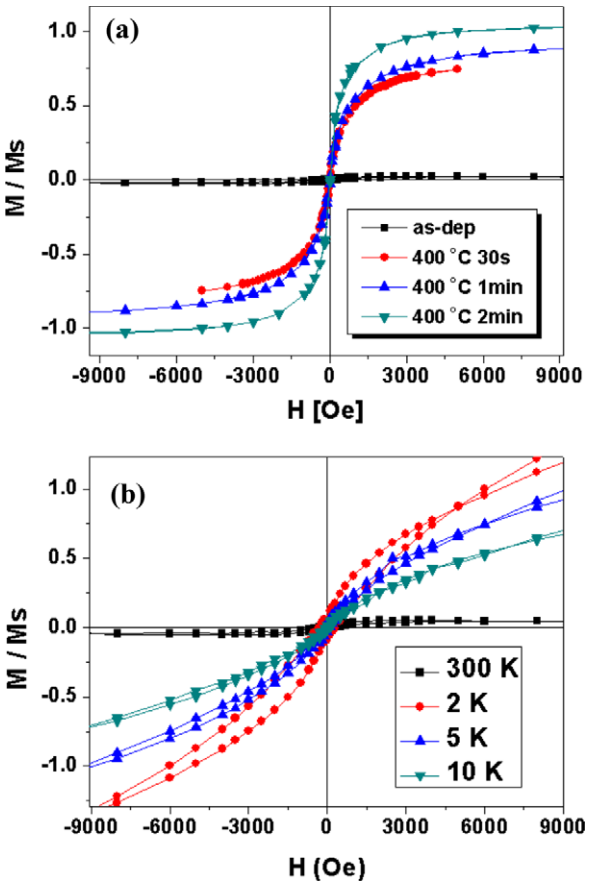

Figure 4. (a) Room-temperature hysteresis (M–H) curve of the Ni nanorods at various annealing conditions. (b) Temperature-dependent M–H curves for the as-deposited Ni nanorods. Curves were measured with the magnetic field (H) applied parallel to the rod axis. M/M_s indicates the magnetization (M) normalized to the saturated value (M_s). Here, M_s was taken from 400 °C, 2 min for (a), and 2 K for (b), respectively, both at $H = 6000$ Oe.

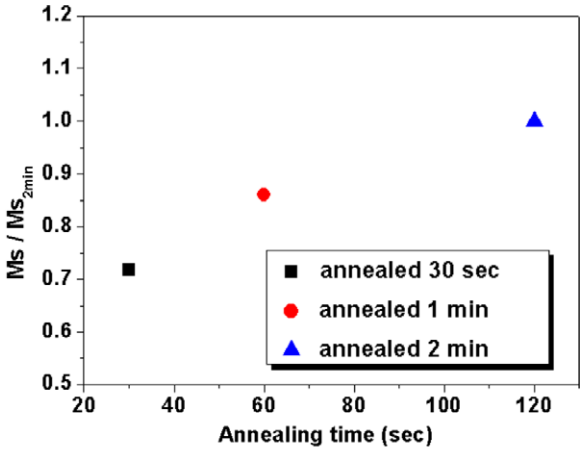

Figure 5. $M_s/M_{s(2\ min)}$ of the Ni nanorods as a function of annealing time. M_s for each one was taken at an applied field of 5000 Oe at room temperature and normalized to that of the 2 min sample.

3. Results and discussion

Figure 1(a) shows the surface morphology of the AAO template prepared in this work, and its inset depicts the enlarged image of the nanopores. The pores have a diameter of about 70 nm and are ordered in a nearly hexagonal pattern with a uniform density of $\sim 3 \times 10^{10}$ pores cm^{-2}. Figures 1(b) and (c) present surface and cross-sectional SEM images of Ni nanorods, respectively, that were taken after the removal of the AAO template from the Si substrate. As shaped by the AAO, Ni nanorods were constructed with a dimension of ~330 nm in height and ~70 nm in diameter (aspect ratio = ~4.7).

The cross-sectional and plan-view transmission electron microscopy (TEM) images of the as-deposited Ni nanorods, shown in figures 2(a) and (b), respectively, reveal important information about their microstructure and growth manner. The results show that the rods are composed of a columnar structure that commences growth along the AAO walls and merges at the center of the pores, with an average diameter of ~25 nm. The HRTEM image shown in figure 3 indicates that the columnar structure contains several nanocrystalline grains with an average size of ~2–3 nm, as highlighted, with the grains having random orientation and embedded in an amorphous matrix [23]. The fact is also supported by the TEM selected area electron diffraction (SAED) pattern, as depicted in the inset of figure 3(b), and the diffusive ring corresponding to Ni {111} planes confirms the existence of the nanocrystalline structure. The microstructure results, especially the size order of the nanocrystalline grains, are similar to those found by Tsai *et al* [23] when using a plating bath with pH = 4.8 and 5.2. It is believed that the nanocrystalline structure is attributed to the addition of P atoms during electroless plating [23].

Figure 4(a) presents the magnetic hysteresis curves of the Ni nanorods with the field applied along the rod axis under various annealing conditions. Interestingly, the as-deposited sample exhibits nearly zero magnetization (M) with an applied field of ~6000 Oe. This is distinct from that observed with electrodeposition patterned with fully saturated magnetization (M_s) under even smaller field application [11, 12, 14, 16, 19]. Surprisingly, the suppressed magnetization of the as-deposited sample was greatly enhanced by application of heat treatment, and the materials followed a ferromagnetic hysteresis curve, indicating an unusual magnetic phase transition as a result of the heat treatment. To verify the magnetic phase of the as-deposited sample, temperature-dependent SQUID measurements were carried out. As highlighted in figure 4(b), the low-temperature hysteresis curve displays ferromagnetic features such as a larger coercive field (H_c) and remnant magnetization. These features gradually disappear with the increase of temperature, and the hysteresis curve eventually becomes nearly linear at higher temperature, suggesting that the magnetic phase is strongly subject to thermal instability. We correlate this phenomenon to the nanocrystalline structure obtained in figure 3 and conclude that the phase is superparamagnetic as a result of the size reduction of ferromagnetic crystallites [10, 27–34]. The size order of nanocrystalline grains (2–3 nm) reported here has been demonstrated as superparamagnetic in a Ni thin film system [35]. In particular, the exchange length λ_{ex} for ferromagnetic metals is in the range of 6–20 nm [36, 37]. Our

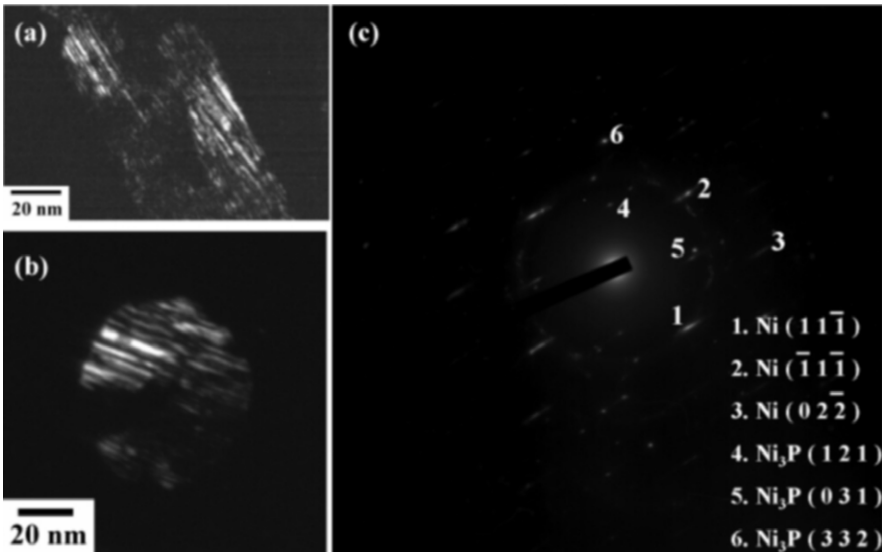

Figure 6. (a) Dark-field TEM images of Ni nanorod annealed at 400 °C for 1 min, taken (a) parallel and (b) perpendicular to the rod axis. (c) SAED pattern taken from (a), showing elongated spots as a result of the laminar structure. Different NiP phases are also presented in the SAED.

size order is much smaller than the ferromagnetic exchange length; therefore, the magnetic moments can randomly flip direction under thermal fluctuation, resulting in a nearly linear hysteresis curve observed in superparamagnetism [38, 39].

Figure 5 illustrates $M_s/M_{s(2\ min)}$ of the Ni nanorods as a function of annealing time. Here, $M_s/M_{s(2\ min)}$ is defined as the saturation magnetization normalized to that of the 400 °C, 2 min sample. It can be seen that the $M_s/M_{s(2\ min)}$ increases with annealing time, showing a value of 0.72, 0.86, and 1.0 for 30 s, 1 min, and 2 min, respectively. The results suggest that the heat treatment not only effectively induces but also enhances the ferromagnetic ordering by increasing M_s by ∼40% from 30 s to 2 min. To further understand the driving force for the obtained superparamagnetic–ferromagnetic transition, dark-field TEM and diffraction spectroscopy were utilized to obtain a better viewpoint to probe the shape and development of the microstructures. Figures 6(a) and (b) present dark-field TEM images of a Ni nanorod that had been annealed at 400 °C for 1 min, taken parallel and perpendicular to the rod axis, respectively. The two images reveal that the Ni nanorod comprises many laminar grains with a thickness of about 2 nm. Figure 6(c) displays the TEM SAED pattern of the same sample. The annealed nanorod consists of two phases, Ni and Ni_3P. As revealed by the diffraction pattern, the electron beam is parallel to both the [011] direction of Ni and the [11$\bar{3}$] direction of Ni_3P. Notably, the elongation of the spots in figure 6(c) confirms the laminar grain structure of the Ni nanorods after annealing. The results demonstrate important information that the superparamagnetic–ferromagnetic transition is attributed to the laminar grain growth driven by the heat treatment. The grains grow parallel to the long axis of a nickel nanorod, together with an increase of the ferromagnetic ordering along the same direction.

Figures 7(a)–(c) are the TEM bright-field micrographs for the samples annealed at 400 °C for 30 s, 1 min, and 2 min, respectively. Figures 7(d)–(f) present the corresponding dark-field micrographs with the same sequence, illustrating the development of the laminar structure. It can be seen

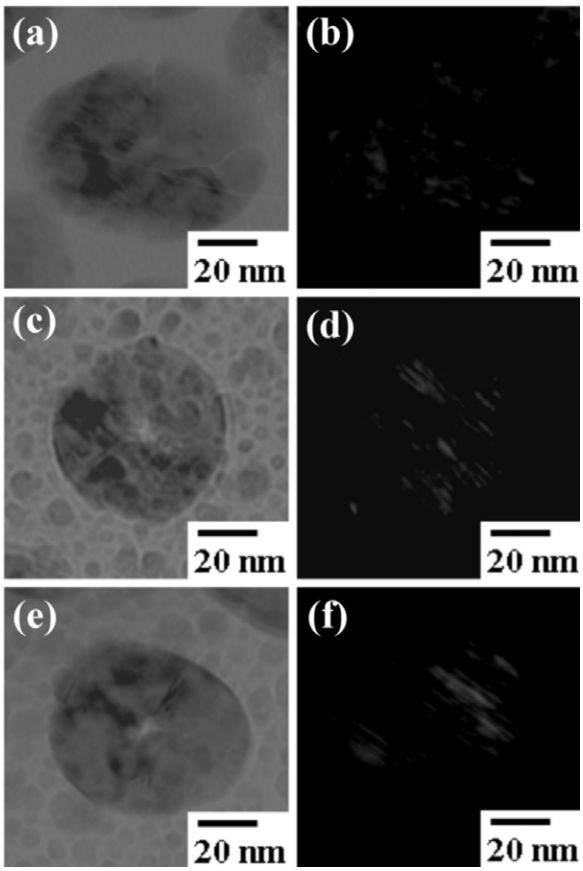

Figure 7. Plan-view bright-field micrographs of the Ni nanorods annealed at 400 °C for (a) 30 s, (b) 1 min, and (c) 2 min; (d)–(f) are the corresponding dark-field micrographs for (a), (b) and (c), respectively.

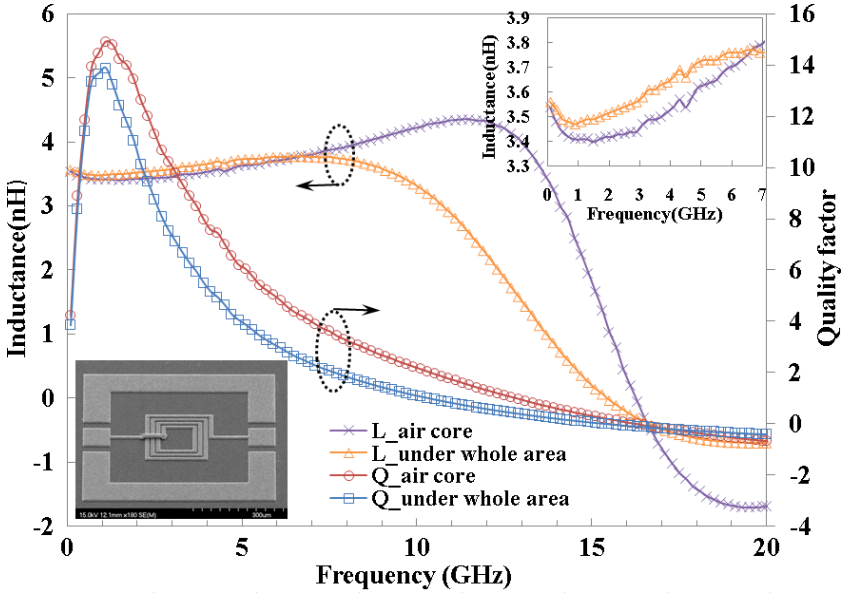

Figure 8. Measurements of high-frequency characteristics for a 3.5 turn spiral inductor. The inset plot on the top right-hand corner is an enlarged view of a high-frequency measurement showing that inductance enhancement can be maintained up to 6.5 GHz. The spiral inductors were fabricated on the Ni nanorods of 400 °C, 2 min condition as shown in the inset SEM image in the bottom left-hand corner.

that the laminar structure is barely formed at 30 s while becoming more complete with increasing annealing time. This can be interpreted as the crystallinity of the Ni nanorods increasing with the increase of heat treatment, serving as the driving force in enhancing the ferromagnetic ordering from within a low crystallinity, superparamagnetic phase. However, one should note that the ferromagnetic curves found in this work (figure 4(a)) exhibit much smaller H_c (∼10 Oe) than those found using electrodeposition (∼200–500 Oe) [40, 41]. We believe that the laminar structure plays a critical role in determining how magnetic moments rotate and ferromagnetic domain walls move, consequently determining the switching mode and value of H_c. Therefore, we argue that the coercive field undergoes a different switching mode than that of the electrodeposited rods with different microstructures (polycrystalline). Alternatively, the application of heat treatment may have removed the material defects formed during deposition. The absence of defects can be thought of as a removal of pinning centers that may hinder the ferromagnetic domain wall motions, thus leading to an effective ferromagnetic rotation, namely, a reduced H_c. However, the mechanism/kinetics for ferromagnetic rotation within a laminar structure are unclear and will require considerable additional efforts.

The formation of the laminar structure of Ni grains is likely caused by the shape of the nanorods. As-deposited electroless Ni is well known to be almost nanocrystalline, and the concentration of P is known to be controlled by the pH of the plating bath [23]. Furthermore, if an electroless Ni film is annealed, the compounds of Ni and P precipitate out, forming crystallized Ni. This study demonstrates that the nano-sized AAO pores may constrain the shape of nanocrystalline Ni grains. The laminar grain structure is herein assumed to be formed because of a preferred growth orientation. Moreover, the preferred orientation of grain growth determines the magnetic properties of the Ni nanorods.

Ni nanorod arrays may be suitable for inductors in high-frequency applications [25]. The nanocrystallinity and the incorporation of phosphorus atoms during electroless plating causes the coercivity of the Ni arrays to be much lower than that obtained from pure Ni nanostructures (about 1000 Oe). However, nanorods with a lower coercivity appear to be more effective for use in high-frequency inductors. Therefore, the Ni nanorods that were fabricated using this technique may have potential applications in high-frequency inductors. Figure 8 shows high-frequency measurement results of a spiral inductor of 3.5 turns. The inductor fabricated from the magnetic Ni nanorods in the AAO template, as shown in the inset SEM micrograph, can have inductance enhancement in the GHz range in comparison with that of the inductor without Ni nanorods. The enlarged high-frequency measurement shown on the top right-hand corner of figure 8 indicates that an inductance increase of up to 3%, i.e., 3.58 nH @3 GHz versus 3.47 nH @ 3 GHz, can be achieved and that the enhancement can be maintained to 6.5 GHz. In general, inductors with a ferromagnetic core usually show poor performance at high frequencies, due to the ferromagnetic resonance (FMR) effect and the eddy current loss occurrence in the layer of magnetic material [42]. According to the simplified Landau–Lifshitz–Gilbert equation [44], the FMR frequency of a ferromagnetic film can be calculated as follows:

$$f_{\mathrm{FMR}} \cong \gamma/2\pi\sqrt{H_k(H_k + 4\pi M_s)} \qquad (2)$$

where γ, H_k, and M_s are the gyromagnetic ratio, which is 176 GHz T^{-1}, the anisotropy magnetic field, and saturation magnetization, respectively. The frequency usually falls within the range of several hundred MHz to 1 GHz, which is coincident with the operational frequency range of the

present wireless operational frequencies. Since the FMR effect would result in a large inductance variance in the region neighboring the resonant frequency, such an inductor with a ferromagnetic core is not suitable for RFIC applications. Previous investigations have also shown that the rod-like shape and nanometer size of magnetic material could have a higher anisotropy magnetic field H_k^4. Since the annealed Ni nanorods developed in this work are grown within the anodic alumina oxide (AAO) template, which serves as an electrical insulator and can isolate each nanorod to effectively reduce the eddy current loss in the layer of magnetic materials, the experimental result has shown the feasibility of the Ni nanorods for spiral inductor fabrication.

4. Conclusion

In summary, Ni nanorod arrays were fabricated on a silicon substrate by electroless deposition of Ni onto an AAO template. As-deposited Ni nanorods exhibit superparamagnetic behavior because of their nanocrystalline microstructure. Annealing causes grains to grow into a laminar structure. Simple annealing also permits a controlled transition from superparamagnetic to soft ferromagnetic behavior in nanorods. Since the H_c of annealed nanorods is very low, they have potential as magnetic building blocks in nanoscale devices such as high-frequency inductors.

Acknowledgment

The authors would like to thank the National Science Council of the ROC for financial support through grant No. 94-2623-7-009-007-AT.

References

[1] Whitney T M, Jiang J S, Searson P C and Chien C L 1993 *Science* **261** 1316
[2] Yang B, Zong B and Shen Z 2002 *Nano Lett.* **2** 751
[3] He Y, Fu J, Zhang Y, Zhao Y, Zhang L, Xia A and Cai J 2007 *Small* **3** 153
[4] Cordente N, Respaud M, Senocq F, Casanove M, Amiens C and Chaudret B 2001 *Nano Lett.* **1** 565
[5] Zhou P, Xue D, Luo H and Chen X 2002 *Nano Lett.* **2** 845
[6] Li D, Thompson R S, Bergmann G and Lu J G 2008 *Adv. Mater.* **1** 20
[7] Lee H, Gu G H, Son J Y, Park C G and Kim H 2008 *Small* **4** 2247
[8] Jeong U, Teng X, Wang Y, Yang H and Xia Y 2007 *Adv. Mater.* **19** 33
[9] Kim J, Ni W, Lee C and Kan E C 2006 *J. Appl. Phys.* **99** 08R903
[10] Jung S W, Park W I, Yi G C and Kim M 2003 *Adv. Mater.* **15** 1358
[11] Tian F, Zhau J, Wei D and Shen Y T 2005 *J. Phys. Chem.* B **109** 14852
[12] Xu L, Tung L D, Spinu L, Zakhidov A A, Baughman R H and Wiley J B 2003 *Adv. Mater.* **15** 1562
[13] Cao H, Xu Z, Sang H, Sheng D and Tie C 2001 *Adv. Mater.* **13** 121
[14] Bao J, Tie C, Xu Z, Zhou Q, Shen D and Ma Q 2001 *Adv. Mater.* **13** 1631
[15] Gau D, Fan L, Sang J, Liu Y, Hanh S and Zou X 2007 *Nanotechnology* **18** 405304
[16] Tao F, Guan M, Jiang Y, Zhu J, Xu Z and Xue Z 2006 *Adv. Mater.* **18** 2161
[17] Peng Y, Zhang H L, Pan S L and Li H L 2000 *J. Appl. Phys.* **87** 7405
[18] Valizadeh S, Georg J M, Leisner P and Hultman L 2001 *Electrochim. Acta* **47** 865
[19] Nielch K, Wehrsophn R B, Barthel J, Kirschber J, Gosele U, Fischer S F and Kronmuller H 2001 *Appl. Phys. Lett.* **79** 1360
[20] Qin D H, Cao L, Sun Q Y, Huang Y and Li H L 2002 *Chem. Phys. Lett.* **358** 484
[21] Sander M S and Tan L S 2003 *Adv. Funct. Mater.* **13** 393
[22] Rabin O, Herz P R, Lin Y M, Akinwande A I, Cronin S B and Dresselhans M S 2003 *Adv. Funct. Mater.* **13** 393
[23] Tsai T K and Chao C G 2004 *Appl. Surf. Sci.* **233** 180
[24] Sorkhabi H A and Rafizadeh S H 2004 *Surf. Coat. Technol.* **176** 318
[25] Han S, Chen H Y, Chen C C, Yuan T N and Shih H C 2007 *Mater. Lett.* **61** 1105
[26] Hsu M C, Chao T Y, Liu C M and Chen C 2009 *IEEE Trans. Nanotechnol.* **8** 281
[27] Sun X, Gutierrez A, Yacaman M J, Dong X and Jin S 2000 *Mater. Sci. Eng.* A **286** 157
[28] Sun X 2003 *J. Dispers. Sci. Technol.* **24** 557
[29] Amekura H, Kitazawa H, Umeda N, Takeda Y and Kishimoto N 2004 *Nucl. Instrum. Methods* B **B224** 114
[30] Liu X, Huang K, Zhou S, Zhao P, Meridor U, Frydman A and Gedanken A 2006 *J. Magn. Magn. Mater.* **305** 504
[31] Marek G, Jorge P J, Benito R G, Marina S, Igor B, Michael F and Luis L M 2008 *Chem. Mater.* **20** 5399
[32] Teong U, Teng X, Wang Y, Yang H and Xia Y 2007 *Adv. Mater.* **19** 33
[33] Wu S H and Chen D H 2003 *J. Colloid Interface Sci.* **259** 282
[34] Gozzi D, Latini A, Capannelu G, Canepa F, Napoletano M, Gmberle M R and Tropeano M 2006 *J. Alloys Compounds* **419** 32
[35] Zhap Z, Wang H, Wang B and Hou J G 2002 *Phys. Rev.* B **65** 235413
[36] Ross C A, Chantrell R, Hwang M, Farhoud M, Savas T A, Hao Y, Smith H I, Ross F M, Redjdal M and Humphery F B 2000 *Phys. Rev.* B **62** 14252
[37] Schabes M 1991 *J. Magn. Magn. Mater.* **95** 249
[38] Neel L 1949 *Ann. Geophys.* **5** 99
[39] Brown W F 1963 *Phys. Rev.* **130** 1677
[40] Nielsch K 2001 *Appl. Phys. Lett.* **79** 1360
[41] Tian F 2005 *J. Phys. Chem.* B **109** 14852
[42] Korenivski V 2000 *J. Magn. Magn. Mater.* **215** 800
[43] Bahl I J 2001 *IEEE Trans. Microw. Theory Tech.* **49** 654
[44] O'Handley R C 2000 *Modern Magnetic Materials* (New York: Wiley)